

Review

Effects of Heat Input on Microstructure, Corrosion and Mechanical Characteristics of Welded Austenitic and Duplex Stainless Steels: A Review

Ghusoon Ridha Mohammed ^{1,2,*}, Mahadzir Ishak ¹, Syarifah N. Aqida ¹
and Hassan A. Abdulhadi ^{1,2}

¹ Faculty of Mechanical Engineering, University Malaysia Pahang, 26600 Pekan, Pahang, Malaysia; mahadzir@ump.edu.my (M.I.); aqida@ump.edu.my (S.N.A.); h.shamary@gmail.com (H.A.A.)

² Institute of technology, Middle Technical University, Foundation of Technical Education, Baghdad-Alzafaranya 10074, Iraq

* Correspondence: Ghusoon_ridha@yahoo.com & PMM_14004@stdmail.ump.edu.my; Tel.: +60-129-457-480

Academic Editor: Robert Tuttle

Received: 19 November 2016; Accepted: 18 January 2017; Published: 30 January 2017

Abstract: The effects of input heat of different welding processes on the microstructure, corrosion, and mechanical characteristics of welded duplex stainless steel (DSS) are reviewed. Austenitic stainless steel (ASS) is welded using low-heat inputs. However, owing to differences in the physical metallurgy between ASS and DSS, low-heat inputs should be avoided for DSS. This review highlights the differences in solidification mode and transformation characteristics between ASS and DSS with regard to the heat input in welding processes. Specifically, many studies about the effects of heat energy input in welding process on the pitting corrosion, intergranular stress, stress-corrosion cracking, and mechanical properties of weldments of DSS are reviewed.

Keywords: duplex stainless steel; heat input; pitting corrosion; intergranular stress; stress corrosion cracking; mechanical properties

1. Introduction

Welding is a fabrication process of generating a perpetual joint result from the melting of the surface of the parts to be joined together, with or without the utilization of pressure and a filler material. In welding, applying heat source defined as the energy input and studying it is essential to study the welding process. Energy input is described as the amount of energy entered per unit length of weld from a moving heat source. The energy input (heat input) is formulated in joules per meter or millimeter. It can be determined as the ratio of total input power in Watts to welding speed. The heat input per unit length (H) is calculated according to the following equation [1]:

$$H = fEI/V \quad (1)$$

where f = Efficiency of heat transfer; E = Volts; I = Amperes; and V = Velocity of heat source (mm/s).

Heat is the controlling factor accountable for thermochemical responses that happen in weld pools, and led upon cooling to modify the chemistry of weld metal. This is confirmed by Sun and Wu [2] when they stated that welding heat input is the key factor impacting heat and mass transfer, liquid flow, and the thermal cycle in the pool.

Stainless steel is recognized as the steel that resists corrosion. This resistance to corrosion is consequent of chromium oxide film created by chromium on the surface of the metal forming a passive layer that isolates and preserves the surface. Austenitic stainless steel (ASS) is widely employed in caustic environments [3–7]. A main downside of ASS is the sensitivity to chloride-induced

stress-corrosion cracking (SCC) [8,9]. Although ferritic stainless steel is more resistant to such corrosion, it is inferior to ASS in terms of ductility and weldability. Given an appropriate composition and thermo-mechanical processing, duplex stainless steel (DSS), which exhibits an austenite–ferrite dual-phase structure, can be obtained. DSS presents many benefits upon single-phase grades, such as increased yield strength and resistance against SCC [10–13].

DSS is a popular constitutional material in the oil, gas, and manufacturing sectors. In particular, DSS is employed in chemical, wastewater, and marine engineering fields, as well as in desalination industries and marine constructions [14–19]. Given the high corrosion resistance of DSS, this material is favorable for shipbuilding, petrochemical, paper, and nuclear industries and can gradually substitute the expensive 300 ASS [20]. DSS is also the preferred material for petroleum and refining industries [21]. The important mechanical properties of DSS help reduce thickness and are especially required in transportation to address the demand of the industry sector [17,22–27].

For the commonly used ASS, the material should be held in the solution-annealed condition for optimal corrosion resistance. As such, weld thermal cycles are selected to ensure rapid cooling of the weld metal and the adjacent Heat-Affected Zone (HAZ), thereby preventing the formation of deleterious phases, which can adversely affect the corrosion properties [28,29]. Consumables should be selected to ensure the proportion of 5% to 10% delta ferrite in the welded microstructure, which is primordial to inhibit solidification cracking. The heat input and temperature are limited to a maximum of 1.5 KJ/mm and 100 °C, respectively, to avoid extensive precipitation of brittle phases in weld metal when very slow cooling is applied.

Directions for welding technologies indicate that excessive dilution with the base metal should be avoided [30]. Basically, instructions to weld DSS are recommended on the expertise with ASS. Thus, when high heat inputs and slow cooling rates are applied (Figure 1), the properties of DSS weldment can accurately advance [31].

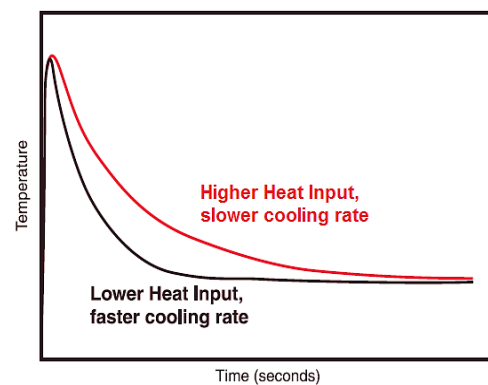


Figure 1. Heat input influences cooling rate [32].

This review does not aim to specify the welding conditions for DSS, but rather to draw attention to the difference in transforming behavior between ASS and DSS and consequently determine how this difference was affected by heat input. Therefore, this review highlights the differences in the physical metallurgy between ASS and DSS and discusses the existing works about the weldment properties of DSS.

2. Metallurgy

2.1. Duplex Structure

DSS consists of ferrite and austenite compounds. Table 1 presents the typical compositions of the common DSS. Many other grades of DSS exist, but most of them would fall in the same compositional

range (Table 1). Clearly, a wide range of composition exists, extending from 2101 LDX to the super DSS 2507 [33]. A pseudo-binary phase diagram for Cr and Ni with 70% Fe is illustrated in Figure 2.

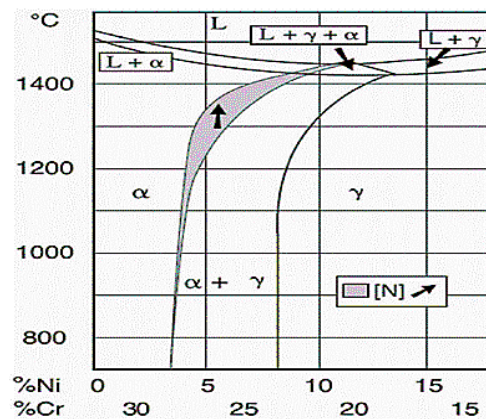


Figure 2. Pseudo-binary Fe-Cr-Ni phase at 70% Fe section illustrating areas of detrimental phase formation [34].

The composition of a representative DSS falls in the $(\alpha + \gamma)$ phase field. For many stainless steel compositions, the austenite phase is expanded; hence, the ferrite phase is separated into high and low-temperature ferrites, which are denoted as delta ferrite and alpha ferrite (formed by the transformation of austenite), correspondingly. Ferrite exists continuously from solidification to room temperature for DSS, and such ferrite is denoted as alpha ferrite. Given that $\alpha/(\alpha + \gamma)$ and $(\alpha + \gamma)/\gamma$ phase boundaries are not vertical, the ferrite-to-austenite ratio in a particular grade would depend on the exact composition, as well as the thermo-mechanical processing [35–37].

Table 1. Typical compositions (in % atom fractions) of some commonly used duplex stainless steels [38]. LDX (Lean Duplex); DX (Duplex); EN (European standard); No. (Number); UNS (Unified Numbering System for Metals and Alloys).

Grade	EN No./UNS	Type	Approx. Composition					
			C	Cr	Ni	Mo	N	Mn
2101 LDX	1.4162/S32101	Lean	0.04	21.0–22.0	1.35–1.70	0.3–0.8	0.2–0.25	4–6
DX 2202	1.4062/S32202	Lean	0.03	21.5–24.0	1.0–2.8	0.45	0.18–0.26	2.0
2304	1.4362/S32304	Lean	0.03	21.5–24.5	3–5.5	0.05–0.6	0.05–0.2	2.5
2205	1.4462/S32205	Standard	0.03	22–23	4.5–6.5	3.0–3.5	0.14–0.2	2.0
2507	1.4410/S32750	Super	0.03	24–26	6–8	3–5	0.24–0.32	1.2

Most modern DSS are designed with a similar austenite-to-ferrite ratio. As a result of the duplex microstructure, partition of alloying components occurs among the phases. Notably, the solidification method of DSS is definite from that of ASS with remaining delta ferrite. Generally, the microstructure of (American Iron and Steel Institute) AISI 304 ASS is completely austenitic at room temperature. In the process of regular welding, the cooling rate is accelerated; thus, the ferrite–austenite alteration cannot be completed, and some δ -ferrite is kept at room temperature after solidification. High input heat leads to a low cooling rate, which further contributes to the change from delta-ferrite phase to austenite phase in weld metal with stainless steel [39–41]. Consequently, the duplex $\delta + \gamma$ structure will be the definitive composition of the weld metal of ASS [42–45].

In the phase equilibrium, the influence of various alloying elements can be quantified by employing equivalent amounts of Ni and Cr. For a very long time, many equations have been used to calculate these two equivalent amounts [46–48]. The Schaeffler diagram [46] and the DeLong

diagram [47] shown in Figure 3 are possibly the most commonly used approaches to calculate the ferrite contents in stainless steel weld metals. The equations reported by Datta [49] are listed below:

$$Cr_{eq} = 1.5(Mo) + (Cr) + 5.5(Al) + 5(V) + 2(Si) + 1.75(Nb) + 1.5(Ti) + 0.75(W) \quad (2)$$

$$Ni_{eq} = (Co) + 0.3(Cu) + 0.5(Mn) + (Ni) + 30(C) + 25(N) \quad (3)$$

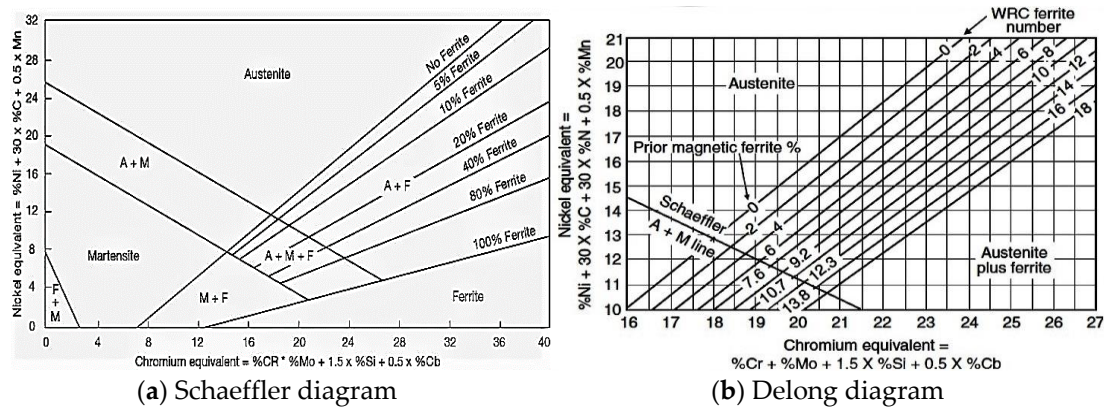


Figure 3. Constitution diagrams to predict phase content in stainless-steel weld metal from chemical composition: (a) Schaeffler diagram [46]; and (b) Delong diagram [47].

These equations have also been previously discussed in detail for stainless steel welding [50,51]. The literature indicated that a Schaeffler alloy with a Cr_{eq}/Ni_{eq} ratio under 1.48 would stabilize essentially as austenite; moreover, delta ferrite is formed from the chromium- and molybdenum-enriched residual melts between the austenite cells or dendrites. As expected, this delta ferrite would be enriched in Cr and Mo.

When the alloy presents a Cr_{eq}/Ni_{eq} ratio between 1.48 and 1.95, primary solidification occurs in the ferrite–austenite mode. This process also results in the segregation of alloying elements upon solidification, with the gamma and alpha phases enriched in austenite- and ferrite-forming elements, respectively. For steels of Cr_{eq}/Ni_{eq} ratio, the remaining ferrite can also undergo solid-state transformation to austenite. Weldments of DSS with a Cr_{eq}/Ni_{eq} ratio above 1.95 stiffen as a single-phase ferrite.

With the high diffusivity of Cr and Mo in ferrite, the ferrite solidification is not accompanied by significant segregation. The austenite is formed from the solid-state ferrite via a Widmanstätten mechanism [51]. Segregation of ferrite stabilizers to alpha, and of austenite stabilizers to gamma, occurs during the solid-state transformation but not during solidification when the Cr_{eq}/Ni_{eq} ratio is less than 1.95. Given this solid-state segregation, the phase balance and amount of segregation will be controlled by factors including the cooling rates for castings and weldments, whereas the thermo-mechanical processing conditions and annealing treatment are very important for wrought products. Additionally, the solidification of duplex weldments occurring in the single-phase ferritic mode largely influences the precipitation of other phases [52–54].

2.2. Precipitation of Other Phases

As the outcome of DSS and super DSS (SDSS) thermal history, one of the significant concerns to gain the required mechanical performance and resistance to corrosion is to understand their microstructural evolution. Derivation of the time–temperature history of the occurrence in welding processes or treatments of technical heat might lead to the deposition of various compounds (e.g., Cr_2N) and a few other intermetallic phases (e.g., σ phase) as illustrated in Figure 4a,b. Such microstructural characteristics are often related to harmful effects on the corrosion resistance, as well as the mechanical behavior of the steel [55]. In fact, σ phase deposition can devalue the corrosion features, in which Mo

and Cr are retained in this phase. Moreover, such deposition can reduce the toughness of DSS and SDSS [56–60].

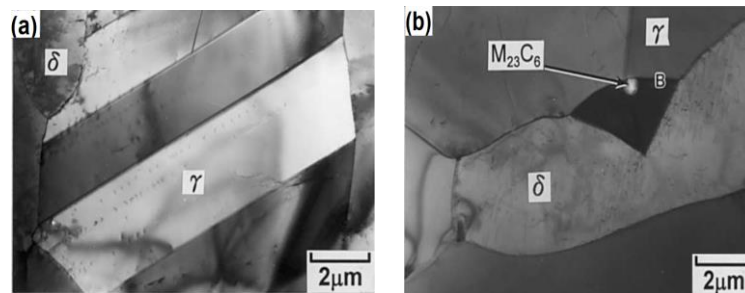


Figure 4. Transmission electron micrograph of duplex stainless steel: (a) as received; and (b) image of σ phase contained with a $M_{23}C_6$ carbide particle after solution treated at 1080 °C [58].

High toughness can be obtained by implementing suitable solution temperatures and cooling rates [61–63]. This finding is consistent with a previous report [64] indicating that the optimal solution temperature and cooling rate result in high toughness. In addition to austenite and ferrite, other phases may occur depending on the thermal history of the steel, when DSS is exposed to a temperature range of 300 to 1000 °C [65–68]. Examples of such phases are chromium nitrides, carbides, or carbonitride, as well as gamma-phase, chi-phase, R-phase, alpha-prime precipitation, [69–72], alpha precipitation, copper precipitates, and martensite in gamma phase. Generally, the formation of secondary phases influences the corrosion resistance and mechanical properties [73]. The absence of these phases is a result of the rapid cooling in the weld zone and prompt growth and nucleation compared with the fusion process [74]. The temperature–time precipitation curves for various phases observed in a 2205 type alloy are shown in Figure 5.

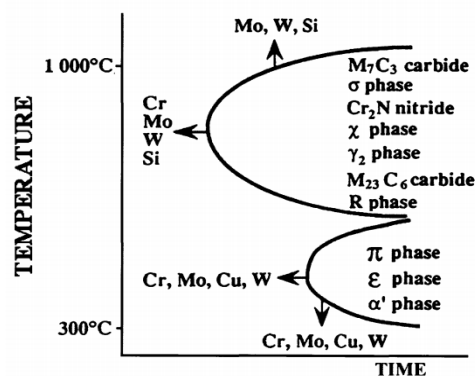


Figure 5. Isothermal cooling curve for the ternary Fe-Cr-Ni system showing the effect of alloying addition on the precipitation of the secondary phases that can form upon cooling [75].

Most of the modern DSS are rich in nitrogen (0.1% to 0.2%). Nitrogen, an austenite stabilizer, is added as both a solid-solution hardener and resistance promoter against pitting corrosion in chloride-containing media. As previously reported, chromium nitrides precipitate in the ferritic phase when a DSS is quenched from a very high annealing temperature [76–78]. Chromium nitrides precipitated when rapid cooling occurred in weld metal or the HAZ of welded DSS [78–81]. Furthermore, fine Cr_2N precipitates were observed when worked on the rod of UNS S31803 DSS treated in two stages [82], that is, after treatment at 1050 °C for 1 h and then at 800 °C from 100 to 31,622 min, with water as a quenching medium for the two stages.

Nevertheless, whether the regulating action is the nucleation rate remains incompletely understood [28,58,83], although the growth kinetics of this response have been widely investigated [84,85]. The amount of Cr_2N precipitation increases with the rise of annealing temperature. As the annealing temperature increases, the volume fraction of austenite decreases, and the ferrite must take up more nitrogen in the solid solution. Although these levels of nitrogen are soluble in ferrite at high temperatures, Cr_2N precipitates in the ferrite upon rapid cooling because nitrogen is relatively insoluble in ferrite at low temperatures. For weldments, the same mechanism is operative, and the HAZ regions were heated to 1300 °C and higher, at which the steel subsisted wholly ferritic with nitrogen in the solid solution. The degree of sensitivity is associated with the great supplement of Cr and Mo drain region outcome from intermetallic phases.

Under certain welding conditions, this region can experience a very rapid cooling cycle, and severe Cr_2N precipitation occurs in an almost completely ferritic HAZ. If the HAZ experiences slower cooling, austenite is formed and nitrogen is dissolved in the austenite, thus reducing the amount of Cr_2N precipitation. Additionally, the cooling rate has been proven to decline as the interpass temperature increases [86].

For ASS, the heat input should be reduced to accelerate the cooling time in the weld metal and the adjoining HAZ, thereby ensuring that deleterious phases, such as M_{23}C_6 , do not precipitate during the welding process [87]. By contrast, very low heat inputs can disastrously affect the renitence of DSS welding against pitting corrosion [88].

3. Properties of Duplex Stainless Steel Weldments

3.1. Pitting Corrosion

El-Batahgy et al. [89] studied the influence of laser welding parameters (simultaneous heat inputs and shielding gas) on the corrosion resistance of autogenously bead-on plates; their results affirmed that the corrosion average of plates combined contracts with the rise in welding speed, indicating the drop in heat input. This effect of heat input can be justified by the cooling time [21,90]. When the welding process occurs with less heat input, the rapid cooling time leads to a scant measure of austenite and major chromium nitride precipitation.

The above phenomenon can drive consumption of Cr, N_2 all over the residue, which causes a harmful result on the pitting impedance. The use of N_2 as a shielding gas to substitute argon, below similarly stream situation, has also resulted in an exceptional reduction in corrosion speed of connecting pieces. This finding is supported by Srinivasan [91] and Lothongkum [92] and advances the corrosion characteristics of laser joint parts manufactured with nitrogen as a shielding gas relevant to improve the ferrite–austenite ratio in weld metal WM and HAZ. The corrosion morphology of grains around precipitates and the precipitate-free zone were left intact and clarified on the substructure of the chromium exhaustion around the Cr_2N precipitates in ferrite.

Slow cooling rates permit enough time for restoration (Cr redistribution) of the depleted zones around the Cr_2N precipitates. This phenomenon is considered a beneficial effect from high heat inputs. Yasuda et al. [93] studied the influence of heat input on the resistance of a 2205 alloy against pitting corrosion. HAZs were then simulated by heating the samples of 2205 alloy to varying temperatures, quenching in water and in compressed air, and then by air cooling to yield cooling rates of 300 °C/s, 40 °C/s, or 20 °C/s.

Cr_2N was identified in the ferrite phase after cooling at fast and slow rates. Therefore, the beneficial effect of slower cooling rates on resistance against pitting corrosion was explained by the restoration of Cr-depleted areas nearby residues. Higher austenite volume fractions taking more nitrogen into solid solution with a subsequent decrease in the amount of Cr_2N precipitated in ferrite may also contribute to the beneficial effect of slow cooling rates. In terms of weld heat input, the heat inputs greater than 1 kJ/mm can improve the pitting resistance.

Plasma arc welded 2304 DSS was investigated in terms of pitting corrosion resistance by using Cr_{eq}/Ni_{eq} ratio; the results revealed that the microstructure is more balanced with austenite phase after thermal cycles with low Cr_{eq}/Ni_{eq} , and the pitting corrosion resistance decreased with the increase of Cr_{eq}/Ni_{eq} [94]. Moreover, high heat input and satisfactory time intended for ferrite–austenite transformation produce superior austenite content, and heat input plays the main role in the corrosion resistance and microstructure of DSS joints. This finding clearly explains that heat input is directly related to the strength and metallurgical aspects of DSS [31,95,96].

In addition, Lundquist et al. [97] studied the effects of welding conditions on the resistance of 2205 [85,98] and 2304 DSS against pitting corrosion. The influence of heat input from 0.5 to 3.0 kJ/mm was examined for Tungsten Inert Gas (TIG) welded bead-on-tube welds with and without the addition of a filler metal. The pitting resistance was remarkably improved with increasing heat input (Table 2). The only weld beads made with the highest heat input of 3.0 kJ/mm passed the $FeCl_3$ test for duplicate specimens. At 25 °C, welds made by heat input of 2.0 kJ/mm by using filler metal and at 2.5 kJ/mm were autogenously resistant to pitting. When a filler metal is used, lower heat inputs can be tolerated without affecting the resistance against pitting corrosion. The reason for the detrimental effect of low heat inputs was also attributed to an appreciable amount of Cr_2N precipitation in ferrite grains. The amount of precipitation diminished for higher heat inputs was virtually absent at 3.0 kJ/mm. This finding can be explained by the austenite reformation at the expense of nitride precipitates.

In addition to TIG welding, Lundqvist et al. [97] also performed Shielding Metal Arc (SMA) butt welding on 20 mm-thick 2205 plate by using heat inputs from 2.0 to 6.0 kJ/mm. Although the entire top surfaces of the weld metal passed the pitting test in 10% $FeCl_3$ 6HP at 30 °C irrespective of heat input, the weld metal on the root side, which was the first to be deposited, failed. To further investigate this phenomenon, tests on critical pitting temperature were conducted under 3% NaCl.

Table 2. Pitting tests on TIG-welded bead-on-tube welds of 2205 X/2 = Specimens attacked/specimens tested solution: 10% $FeCl_3 \cdot 6H_2O$.

Filler Metal	Temperature (°C)	Heat Input, kJ/mm					
		0.5	1.0	1.5	2.0	2.5	3.0
Sandvik	25	-	2/2	2/2	0/2	0/2	0/2
22.8.3.L	30	-	2/2	2/2	2/2	1/2	0/2
None	25	2/2	2/2	2/2	2/2	0/2	0/2
	30	2/2	2/2	2/2	2/2	1/2	0/2

Critical pitting temperatures of 48, 43 and 40 °C were obtained at heat inputs of 2.0, 4.0 and 6.0 kJ/mm, correspondingly. Microstructural evaluation revealed that extremely fine austenite precipitated in the first- and second-weld beads. A higher heat input during subsequent weld passes led to a reformation of more austenite. In addition to nitrides, fine precipitates of austenite, which were presumed to be reformed at temperatures as low as 800 °C, also negatively affected the pitting resistance. However, the reformed austenite is less detrimental to pitting resistance than Cr_2N precipitates. Lundquist et al. also investigated the use of nitrogen as a shielding gas. Although nitrogen provides adequate protection against oxidation, nitrogen also diffuses into the weld metal and HAZ. Such diffusion increases the amount of austenite in the root run and effectively suppresses the amount of chromium nitride precipitated, which can possibly enhance the resistance to pitting corrosion.

It is generally agreed that very low heat inputs should be avoided on DSS and that much higher heat input can be tolerated for austenitic. This affects the costs of weld fabrication since joints can be made in fewer passes [99]. It should be noted that heat input alone does not determine the cooling rate, but that thickness of the parent metal and interpass temperatures also should be considered. The heat inputs for SAF 2304 and SAF 2205 are specified to be 0.5 to 2.5 kJ/mm, respectively, with the upper

limit not considered [97,100]. The choice of heat input pertinent with the material thickness, as the reform of sufficient austenite, needs heat inputs in the upper part of the thick material.

Jang et al. [101] refer to the influence of shielding gas component using N_2 on the impedance to pitting corrosion at the Hyper Duplex Stainless Steel HDSS within quiet massive chloride environment. After welding, the resistance of the HDSS tube to pitting corrosion was produced using N_2 with Ar shielding gas and was increased due to the decrease of α -phase in the HAZ and weld metal. Furthermore, the improved corrosion resistance is assigned to the reduction of Pitting Resistance Equivalent Number (PREN) variation between the α -phase and γ -phase in the weld metal [16,102].

Furthermore, Wang et al. [103] used dissimilar metals to investigate the consequence of welding conditions in terms of welding process type. Gas Tungsten Arc Welding (GTAW) joint A and Shielded Metal Arc Welding (SMAW) joint B were applied sequentially, and ER2209 welding wire was used to join two different materials: 2205 DSS and 16MnR low alloy high-strength steel. To assess the corrosion resistance of weld metal, the plates were partly tightened with A/B glue and a corrosion mixture of 3.5% NaCl. Figure 6 and Table 3 present the results of electrochemical corrosion experiments with 2205 DSS base metal and weld metal, correspondingly. However, their corrosion possibilities are relatively uneven: joint B < joint A < 2205 DSS. The corrosion possibility is a constant index of electrochemical corrosion renitency and exhibits the sensitivity to corrosion of the material [77,91,104].

Table 3. Electrochemical parameters of DSS BM and weld metals [103]. DSS: duplex stainless steel. BM: Base Metal.

Samples	Joint A	Joint B	DSS BM
Corrosion potential/ E_{corr} (V)	−0.394	−0.463	−0.251
Corrosion current/ I_{corr} (A)	0.2932	0.3041	0.2862

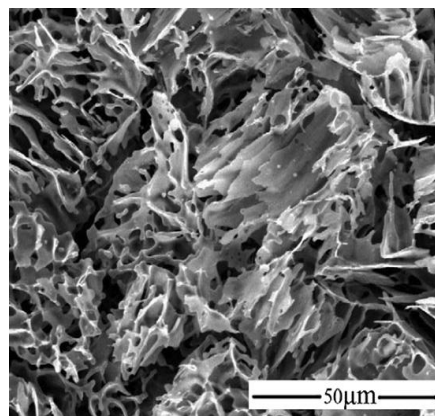


Figure 6. Scanning electron microscopy (SEM) micrograph of pitting corrosion.

The weld metal of DSS is more resistant to pitting corrosion than the base metal. Furthermore, the enhanced response of weld metal to pitting resistance is associated with the addition of Cr and Ni elements [105]. This finding is supported by Olsson [106], who reported that the stability of passive films gained from Cr and Ni would reduce the comprehensive decay of Fe and Cr. Overall, the weld microstructure is influenced by the differences in the heat input between joint A and joint B and leads to change in the configuration state of the element surface unfavorable layer.

For the common DSS 2205, its composition range was considered as UNS S31803. However, the N content associated with UNS S31803 may be reduced to 0.08%, and a plane is assured to be minimized for reliable HAZ and autogenous fusion zone properties in the same status of the welding process. In addition to the increased requirement of minimum nitrogen for S32205 versus

S31803, the minimum Mo and Cr contents are enhanced. During welding, nitrogen controls the ferrite/austenite phase equality [107].

Susceptibility to solidification cracking is one of the problems coupled with fusion welding of these materials, which is comparatively higher than that of 304L ASS [108]. Nitride precipitation was noted in HAZ. The presence of δ -ferrite with higher Cr content may deleteriously affect the corrosion resistance because of the potential difference between the δ -ferrite and austenite phases [109], but this factor may exert less influence on the corrosion resistance than the others. The corrosion properties of the welds also include grain boundary effects [110,111]. Experimentally, Shamanian and Yousefieh [112] studied the differences in heat input result on a DSS, a microstructure of UNS S32760 in seawater. Remarkably, the heat input at about 0.95 kJ/mm presents the largest component of corrosion, that is, the lack of harmful phases resulting in sigma and Cr_2N , as well as the attribution of equal ferrite–austenite.

The GTAW process pulsed current has benefited the representative GTA process, that is, the ferrite–austenite ratio within the base metal and weld metal relies on the welding energy input. After welding in DSS pipes of four distinct sizes, metallography tests completed by scanning electron microscopy (SEM) and energy-dispersive X-ray spectroscopy (EDX) were conducted to show the phases of chemical compositions presented in the microstructure, and polarization curves of various specimens were analyzed. As a result, the formation of sigma and Cr_2N phases decreased the potential formation of corrosion for a fine and coarse structure in the weld metal. The undercooling level will be prospected within a welding process, given that in the cap region, the weld metal will chill down more rapidly because of lower ambient temperatures at the weld surface and adjacent parent material at the beginning. No evidence shows the existence of secondary austenite (γ'), which is present in all of the examined weld metal conditions. Furthermore, areas containing the intermetallic phases of any of the generally prospected carbides were not observed [113].

The detrimental effects of very high heat inputs or multi-pass welding are the formation of secondary austenite and Cr_2N in the HAZ. Interestingly, the number of thermal cycles is one of the most related criteria to estimate the deleterious effect of sigma phase development, as previously reported [99,114,115].

3.2. Intergranular Corrosion

At grain boundaries, the precipitation of the chromium carbides causes susceptibility to intergranular corrosion, which can be a serious problem in ASS if these materials are held for prolonged periods in the sensitization region (about 500 to 750 °C) [116–118]. This kind of corrosion occurs from the Cr deficiency nearby M_{23}C_6 precipitates. As for combating intergranular corrosion in stainless steels, one way is to reduce carbon content below 0.3% to delay the deposition of M_{23}C_6 , which helps to avoid any damaging consequence.

One of the exceptional features of DSS is the resistance against sensitization. The ferrite phase provided the largest amount of Cr in carbides as a result of high diffusivity of Cr and the high Cr content in the ferrite phase. Accordingly, an extremely broad Cr-consuming region dwells at the ferrite part of the interface. The austenite phase offered a really scanty Cr volume, leading to a very thin but penetrating Cr-consuming region on the austenite side of the interface [82]. Intergranular corrosion in HAZ decreased with the increasing number of weld passes. According to the results, as the number of passes increased, the corrosion attack of grain boundaries decreased. This behavior is ascribed to the prolonged retention time above the sensitization temperature range, which promotes the solubilization of chromium carbides in the grain matrix, thereby avoiding sensitization [119].

The elegant resistance of duplex alloys against sensitization is achieved by recharging the small region with diffusing Cr from the inside of the austenite grain. Despite this inherent resistance, many commercial DSS contain less than 0.03% carbon, thus further reducing the risk of sensitization. In addition to the effect of heat input on the pitting corrosion of DSS weldments as previously detailed,

Sridhar [78] and Lundquist [97] studied the effect on resistance to intergranular corrosion. In both cases, excellent resistance was reported, even in the case of high heat inputs.

For the resistance against intergranular corrosion and SCC, no detrimental effect from high heat inputs was found. The tensile elongation and toughness of welds on DSS are affirmed to increase when the heat input is raised.

3.3. Stress-Corrosion Cracking

DSS demonstrated desirable impedance to SCC. DSS is not as resistant as ferritic SS but more resistant than austenitic against SCC [15]. The susceptibility of DSS to SCC depends on many factors, including alloying elements [120,121], microstructures [122,123], applied stresses [124,125], and environment [126–129].

Slow-strain rate tests ($2.2 \times 10^{-6} \text{ s}^{-1}$) at 35% boiling water MgCl_2 solution and 125 °C were performed to determine the sensitivity to SCC [98]. Additional tests in an inoperative environment (glycerin) were conducted. All specimens with welded joints tested in glycerin at 125 °C showed sufficient plasticity, and their fracture surfaces were entirely ductile. Detailed examinations revealed that these samples broke in parent material 316L steel close to HAZ of the weld. Samples tested in MgCl_2 solution broke in a brittle manner. The welded specimens were brittle or mixed, and the ductile-brittle shape of fracture surfaces. Thus, the consequence of SCC is this succession of plasticity [130].

The ways of crack diffusion ordinarily continue together with state limits or transverse ferrite grains. Cracks were frequently prevented on extended, upright austenite grains, or overpass through [131]. The heat input did not influence the susceptibility to SCC.

3.4. Mechanical Properties

The ferrite content of DSS can considerably influence the yield strength, tensile ductility, and toughness of the alloy [89,97,112,132]. As such, it further assumed that the heat input will manipulate these properties in a welded part because the austenite-to-ferrite stability is related to the cooling rate [133]. The toughness was reportedly improved as the heat input was top-up on SAF 2205 [97]. This finding was further correlated to the reduction of ferrite content. They also point out that sigma phase and 475 °C embrittlement are not troubled when welding modern DSS, owing to well-balanced chemical compositions and favorable austenite-to-ferrite ratios. From a strength and toughness viewpoint, the arc powers do not need to be maximized for 2205 [134]. The findings also proved that even 1% of sigma phase formation in DSS is sufficient to cause embrittlement. Furthermore, the coarse-grained ferrite structure formed near the fusion line is responsible for the reduction in impact toughness of the DSS weld [135–137].

For austenite antirust steels, the important relationship between the changes, as well as heat input in microstructural development, is highly related to the relevant mechanical performance in the weldments of AISI 304L stainless steel by GTAW [138]. Moreover, little heat input joints show high ductility and tensile strength, but great heat input joints demonstrate small tensile ductility and strength. The HAZ photomicrographs of these weldments show that grain coarsening influence is inducted, which is inclined to recede the joint part and may thus influence the functional performance of the weld joint in practice. With high heat input, the grain-coarsening degree within this zone is comparatively higher, but a small heat input helps to inhibit the grain growth by subjecting the zone to abrupt heat gradients [139]. Hardness is relatively small along the large weld zone of heat input, which includes long dendrites with larger interdendritic spacing, but hardness is improved along with the small weld zone of heat input, which contains comparatively few dendrites along with smaller interdendritic spacing. All HAZs in distinct weldments undergo grain coarsening, of which the extent is increasingly enhanced with the improvement of welding heat input.

Mourad et al. [140] studied the effects of gas tungsten arc as well as laser beam welding on 2205 properties of DSS. The effects of gas tungsten arc welding and beam welding of carbon dioxide

laser on the microstructure and size of fusion zone, mechanical as well as corrosion properties of DSS grade 6.4 mm-thick 2205 plates were comparatively studied. The ferrite–austenite balance of both HAZ and weld metal are affected by heat input, which is a welding process function.

The impacts of heat input on the mechanical properties of UNS S31803 DSS plates from friction stir welding were studied recently [31]. The fracture morphology, residence of elements, and their distribution on joint zone were comprehensively examined through SEM associated with energy dispersive spectroscopy (EDS). The fracture occurred in the base metal and partially penetrated the weld zone. The fracture occurred in the weld region, and the strength of friction welded joints was reduced than the parent material [86]. The fracture did not expand extensively in the base metal and partly entered the weld zone. The fracture occurred in the weld region, and the strength of the friction-welded joints decreased more than the parent material. No intermetallic phases were detected by X-ray diffraction. Outcomes of tensile strength confirmed that the joint strength can be kept when high heat input was applied. However, at room temperature, toughness declined as the heat input grew. Microhardness was improved with the rise of heat input owing to the grain perfection.

After a detailed literature review, most of the investigations are found to have focused on the effects of heat transfer/heat input on DSS by using various welding techniques. The characteristics of various materials processed after different welding process were also analyzed. Clearly, the irregular heat input variations of various fusion welding on DSS cause drastic changes in phase balance, which needs to be balanced. Knowledge about microstructural evolution of such kind of steels, as well as the result of thermal history, is fundamental to achieve the expected mechanical behavior and corrosion resistance. The time–temperature history, derived from industrial heat treatments or welding processes [141–143], may lead to precipitation of various compounds (e.g., chromium carbides and nitrides) and some other intermetallic phases (e.g., σ phase). The formation of such compounds leads to losses in both corrosion resistance and fracture toughness [144]. However, extensive research is needed to deal with the effects of heat input on DSS welds for in-depth understanding of this phenomenon. Few reports exist on different welding processes of DSS grades. Thus, the full-depth knowledge about heat input throughout the welding process of DSS is notably essential for controlling and improving the welding quality. As such, the current research investigated the effects of heat input on mechanical measures such as tensile strength, Charpy impact toughness, microhardness, metallurgical specifics, and corrosion of DSS welded joints.

4. Conclusions

The amount of heat input in the welding process affects the properties of both DSS and ASS. The final properties depend on the variety of solidification modes and the transformation characteristics of these two alloys, especially the corrosion properties.

The following conclusions can be drawn from this review:

- (1) DSS solidifies in the single-phase ferritic mode, whereas ASS solidifies in the austenitic or austenitic–ferritic mode.
- (2) Austenite phase in weldments of DSS is formed by solid-state transformation, which is strongly affected by the cooling rate.
- (3) The resultant ferrite-to-austenite ratio is dependent on the energy input during the welding process.
- (4) In duplex weldments, low heat inputs result in high volume fractions of ferrite and severe precipitation of chromium nitrides, which adversely affect mechanical and corrosion properties.
- (5) High heat inputs requisite sufficient time in the DSS welding for austenite reformation at high temperature.
- (6) The number of thermal cycles is significantly associated criteria to evaluate the deleterious impact of sigma phase extension.
- (7) Susceptibility to SCC and the resistance against intergranular corrosion did not affect from high heat inputs.

Acknowledgments: The authors are grateful to the Universiti Malaysia Pahang (UMP), Pekan, Malaysia, and Automotive Engineering Centre (AEC), Pekan, Malaysia, for financial support given under GRS 1503107 (GRS/8/2015/UMP).

Author Contributions: Ghusoon and Ishak conceived and designed the Review; Hassan and Aqida analyzed the data; Ishak and Ghusoon contributed reagents/materials/analysis tools; Ghusoon wrote the paper

Conflicts of Interest: The authors declare no conflict of interest. And “The founding sponsors had no role in the design of the study; in the collection, analyses, or interpretation of data; in the writing of the manuscript, and in the decision to publish the results”.

References

1. Jarvis, B.L.; Tanaka, M. 3—Gas tungsten arc welding. In *New Developments in Advanced Welding*; Woodhead Publishing: Witney, UK, 2005; pp. 40–80.
2. Sun, J.; Chuansong, W. The effect of welding heat input on the weldpool behavior in MIG welding. *Sci. China Ser. E Technol. Sci.* **2002**, *45*, 291–299. [[CrossRef](#)]
3. Rondelli, G.; Vicentini, B. Susceptibility of highly alloyed austenitic stainless steels to caustic stress corrosion cracking. *Mater. Corros.* **2002**, *53*, 813–819. [[CrossRef](#)]
4. Rondelli, G.; Vicentini, B.; Sivieri, E. Stress corrosion cracking of stainless steels in high temperature caustic solutions. *Corros. Sci.* **1997**, *39*, 1037–1049. [[CrossRef](#)]
5. Parnian, N. Failure analysis of austenitic stainless steel tubes in a gas fired steam heater. *Mater. Des.* **2012**, *36*, 788–795. [[CrossRef](#)]
6. Betova, I.; Bojinov, M.; Hyökyvirta, O.; Saario, T. Effect of sulphide on the corrosion behaviour of AISI 316L stainless steel and its constituent elements in simulated kraft digester conditions. *Corros. Sci.* **2010**, *52*, 1499–1507. [[CrossRef](#)]
7. Chasse, K.; Raji, S.; Singh, P. Effect of chloride ions on corrosion and stress corrosion cracking of duplex stainless steels in hot alkaline-sulfide solutions. *Corrosion* **2012**, *68*, 932–949. [[CrossRef](#)]
8. Elsariti, S.M. Behaviour of stress corrosion cracking of austenitic stainless steels in sodium chloride solutions. *Procedia Eng.* **2013**, *53*, 650–654. [[CrossRef](#)]
9. Alyousif, O.M.; Nishimura, R. Stress corrosion cracking and hydrogen embrittlement of sensitized austenitic stainless steels in boiling saturated magnesium chloride solutions. *Corros. Sci.* **2008**, *50*, 2353–2359. [[CrossRef](#)]
10. Lo, K.H.; Shek, C.H.; Lai, J. Recent developments in stainless steels. *Mater. Sci. Eng. R Rep.* **2009**, *65*, 39–104. [[CrossRef](#)]
11. Bonollo, F.; Tiziani, A.; Ferro, P. Welding processes, microstructural evolution and final properties of duplex and superduplex stainless steels. In *Duplex Stainless Steels*; John Wiley & Sons, Inc.: Hoboken, NJ, USA, 2013; pp. 141–159.
12. Kiasoz, A.; Gurel, S.; Karaaslan, A. Effect of annealing time and cooling rate on precipitation processes in a duplex corrosion-resistant steel. *Metal Sci. Heat Treat.* **2016**, *57*, 544–547. [[CrossRef](#)]
13. Srikanth, S.; Saravanan, P.; Govindarajan, P.; Sisodia, S.; Ravi, K. Development of Lean Duplex Stainless Steels (LDSS) with Superior Mechanical and Corrosion Properties on Laboratory Scale. *Adv. Mater. Res.* **2013**, *794*, 714–730. [[CrossRef](#)]
14. Alvarez-Armas, I.; Degallaix-Moreuil, S. *Duplex Stainless Steels*; John Wiley & Sons: Hoboken, NJ, USA, 2013.
15. Bhattacharya, A.; Singh, P.M. Electrochemical behaviour of duplex stainless steels in caustic environment. *Corros. Sci.* **2011**, *53*, 71–81. [[CrossRef](#)]
16. Lai, R.; Cai, Y.; Wu, Y.; Li, F.; Hua, X. Influence of absorbed nitrogen on microstructure and corrosion resistance of 2205 duplex stainless steel joint processed by fiber laser welding. *J. Mater. Process. Technol.* **2016**, *231*, 397–405. [[CrossRef](#)]
17. Baddoo, N.R. Stainless steel in construction: A review of research, applications, challenges and opportunities. *J. Construct. Steel Res.* **2008**, *64*, 1199–1206. [[CrossRef](#)]
18. Olsson, J.; Snis, M. Duplex—A new generation of stainless steels for desalination plants. *Desalination* **2007**, *205*, 104–113. [[CrossRef](#)]
19. Chandler, K.A. 3—Marine environments. In *Marine and Offshore Corrosion*; Butterworth-Heinemann: Amsterdam, The Netherlands, 1985; pp. 38–50.
20. Sarlak, H.; Atapour, M.; Esmailzadeh, M. Corrosion behavior of friction stir welded lean duplex stainless steel. *Mater. Des.* **2015**, *66*, 209–216. [[CrossRef](#)]

21. Pekkarinen, J.; Kujanpää, V. The effects of laser welding parameters on the microstructure of ferritic and duplex stainless steels welds. *Phys. Procedia* **2010**, *5*, 517–523. [[CrossRef](#)]
22. El Bartali, A.; Evrard, P.; Aubin, V.; Herenú, S.; Alvarez-Armas, I.; Armas, A.; Degallaix-Moreuil, S. Strain heterogeneities between phases in a duplex stainless steel. Comparison between measures and simulation. *Procedia Eng.* **2010**, *2*, 2229–2237. [[CrossRef](#)]
23. Saha Podder, A.; Bhanja, A. Applications of Stainless Steel in Automobile Industry. *Adv. Mater. Res.* **2013**, *794*, 731–740. [[CrossRef](#)]
24. Cunat, P.J. *Stainless Steel in Structural Automotive Applications*; SAE International: Paris, France, 2002.
25. Hariharan, K.; Balachandran, G.; Prasad, M.S. Application of cost-effective stainless steel for automotive components. *Mater. Manuf. Process.* **2009**, *24*, 1442–1452. [[CrossRef](#)]
26. Pouranvari, M.; Alizadeh-Sh, M.; Marashi, S. Welding metallurgy of stainless steels during resistance spot welding part I: Fusion zone. *Sci. Technol. Weld. Join.* **2015**, *20*, 502–511. [[CrossRef](#)]
27. Dur, E.; Cora, Ö.N.; Koç, M. Effect of manufacturing conditions on the corrosion resistance behavior of metallic bipolar plates in proton exchange membrane fuel cells. *J. Power Sources* **2011**, *196*, 1235–1241. [[CrossRef](#)]
28. Urena, A.; Otero, E.; Utrilla, M.; Munez, C. Weldability of a 2205 duplex stainless steel using plasma arc welding. *J. Mater. Process. Technol.* **2007**, *182*, 624–631. [[CrossRef](#)]
29. Zhong, Y.; Zhou, C.; Chen, S.; Wang, R. Effects of temperature and pressure on stress corrosion cracking behavior of 310s stainless steel in chloride solution. *Chin. J. Mech. Eng.* **2016**, *29*, 1–7. [[CrossRef](#)]
30. Rahmani, M.; Eghlimi, A.; Shamanian, M. Evaluation of microstructure and mechanical properties in dissimilar austenitic/super duplex stainless steel joint. *J. Mater. Eng. Perform.* **2014**, *23*, 3745–3753. [[CrossRef](#)]
31. Mohammed, A.M.; Shrikrishna, K.A.; Sathiya, P.; Goel, S. The impact of heat input on the strength, toughness, microhardness, microstructure and corrosion aspects of friction welded duplex stainless steel joints. *J. Manuf. Process.* **2015**, *18*, 92–106.
32. Funderburk, R.S. A look at input. *Weld. Innov.* **1999**, *16*, 1–4.
33. Lai, J.K.L.; Shek, C.H.; Lo, K.H. *Stainless Steels: An Introduction and Their Recent Developments*; Bentham Science Publishers: Beijing, China, 2012.
34. Cieslak, M.; Savage, W. Weldability and solidification phenomena of cast stainless steel. *Weld. J.* **1980**, *5*, 136s–146s.
35. Tseng, K.H. Development and application of oxide-based flux powder for tungsten inert gas welding of austenitic stainless steels. *Powder Technol.* **2013**, *233*, 72–79. [[CrossRef](#)]
36. Kolenič, F.; Kovac, L.; Drimal, D. Effect of laser welding conditions on austenite/ferrite ratio in duplex stainless steel 2507 welds. *Weld. World* **2011**, *55*, 19–25. [[CrossRef](#)]
37. Medina, E.; Medina, J.M.; Cobo, A.; Bastidas, D.M. Evaluation of mechanical and structural behavior of austenitic and duplex stainless steel reinforcements. *Construct. Build. Mater.* **2015**, *78*, 1–7. [[CrossRef](#)]
38. Alvarez-Armas, I. Duplex stainless steels: Brief history and some recent alloys. *Recent Patents Mech. Eng.* **2008**, *1*, 51–57. [[CrossRef](#)]
39. Nowacki, J.; Łukojć, A. Structure and properties of the heat-affected zone of duplex steels welded joints. *J. Mater. Process. Technol.* **2005**, *164*, 1074–1081. [[CrossRef](#)]
40. Hwang, S.W.; Ji, J.H.; Lee, E.G.; Park, K.-T. Tensile deformation of a duplex Fe–20Mn–9Al–0.6C steel having the reduced specific weight. *Mater. Sci. Eng. A* **2011**, *528*, 5196–5203. [[CrossRef](#)]
41. Betini, E.G.; Cione, F.C.; Mucsi, C.S.; Colosio, M.A.; Rossi, J.L.; Orlando, M.T.D.A. Experimental Study of the Temperature Distribution in Welded Thin Plates of Duplex Stainless Steel for Automotive Exhaust Systems. *SAE Int.* **2016**. [[CrossRef](#)]
42. Hunter, A.; Ferry, M. Phase formation during solidification of AISI 304 austenitic stainless steel. *Scr. Mater.* **2002**, *46*, 253–258. [[CrossRef](#)]
43. Yan, J.; Gao, M.; Zeng, X. Study on microstructure and mechanical properties of 304 stainless steel joints by TIG, laser and laser-TIG hybrid welding. *Opt. Lasers Eng.* **2010**, *48*, 512–517. [[CrossRef](#)]
44. Fu, J.; Yang, Y.; Guo, J.; Ma, J.; Tong, W. Formation of two-phase coupled microstructure in AISI 304 stainless steel during directional solidification. *J. Mater. Res.* **2009**, *24*, 2385–2390. [[CrossRef](#)]
45. Eghlimi, A.; Shamanian, M.; Eskandarian, M.; Zabolian, A.; Szpunar, J.A. Characterization of microstructure and texture across dissimilar super duplex/austenitic stainless steel weldment joint by austenitic filler metal. *Mater. Charact.* **2015**, *106*, 208–216. [[CrossRef](#)]

46. Schaeffler, A. Constitution diagram for stainless steel weld metal. *Met. Prog.* **1949**, *56*, 680–680B.
47. Long, C.; DeLong, W. Ferrite content of austenitic stainless steel weld metal. *Weld. J.* **1973**, *52*, 281.
48. Wegrzyn, T. Delta ferrite in stainless steel weld metals. *Weld. Int.* **1992**, *6*, 690–694. [[CrossRef](#)]
49. Datta, P.; Upadhyaya, G. Sintered duplex stainless steels from premixes of 316L and 434L powders. *Mater. Chem. Phys.* **2001**, *67*, 234–242. [[CrossRef](#)]
50. Suutala, N. Effect of solidification conditions on the solidification mode in austenitic stainless steels. *Metall. Trans. A* **1983**, *14*, 191–197. [[CrossRef](#)]
51. Suutala, N.; Takalo, T.; Moision, T. Ferritic-austenitic solidification mode in austenitic stainless steel welds. *Metall. Trans. A* **1980**, *11*, 717–725. [[CrossRef](#)]
52. Baeslack, W.A.; Duquette, D.J.; Savage, W.F. The effect of ferrite content on stress corrosion cracking in duplex stainless steel weld metals at room temperature. *Corrosion* **1979**, *35*, 45–54. [[CrossRef](#)]
53. Menendez, H.; Devine, T. The influence of microstructure on the sensitization behavior of duplex stainless steel welds. *Corrosion* **1990**, *46*, 410–418. [[CrossRef](#)]
54. Ogawa, T.; Koseki, T. Effect of composition profiles on metallurgy and corrosion behavior of duplex stainless steel weld metals. *Weld. J.* **1989**, *68*, 181.
55. Utu, I.D.; Mitelea, I.; Urlan, S.; Crăciunescu, C. Transformation and precipitation reactions by metal active gas pulsed welded joints from X2CrNiMoN22-5-3 duplex stainless steels. *Materials* **2016**, *9*, 606. [[CrossRef](#)]
56. El Koussy, M.; El Mahallawi, I.; Khalifa, W.; Al Dawood, M.; Bueckins, M. Effects of thermal aging on microstructure and mechanical properties of duplex stainless steel weldments. *Mater. Sci. Technol.* **2004**, *20*, 375–381. [[CrossRef](#)]
57. Ahn, Y.; Kang, J. Effect of aging treatments on microstructure and impact properties of tungsten substituted 2205 duplex stainless steel. *Mater. Sci. Technol.* **2000**, *16*, 382–388. [[CrossRef](#)]
58. Chen, T.; Yang, J. Effects of solution treatment and continuous cooling on σ -phase precipitation in a 2205 duplex stainless steel. *Mater. Sci. Eng. A* **2001**, *311*, 28–41. [[CrossRef](#)]
59. Chen, T.; Weng, K.; Yang, J. The effect of high-temperature exposure on the microstructural stability and toughness property in a 2205 duplex stainless steel. *Mater. Sci. Eng. A* **2002**, *338*, 259–270. [[CrossRef](#)]
60. Wessman, S.; Pettersson, R.; Hertzman, S. On phase equilibria in duplex stainless steels. *Steel Res. Int.* **2010**, *81*, 337–346. [[CrossRef](#)]
61. Sieurin, H.; Sandström, R. Austenite reformation in the heat-affected zone of duplex stainless steel 2205. *Mater. Sci. Eng. A* **2006**, *418*, 250–256. [[CrossRef](#)]
62. Kim, S.K.; Kang, K.Y.; Kim, M.-S.; Lee, J.M. Low-temperature mechanical behavior of super duplex stainless steel with sigma precipitation. *Metals* **2015**, *5*, 1732–1745. [[CrossRef](#)]
63. Bouyne, E.; Joly, P.; Houssin, B.; Wiesner, C.; Pineau, A. Mechanical and microstructural investigations into the crack arrest behaviour of a modern $2\frac{1}{4}$ Cr-1 Mo pressure vessel steel. *Fatigue Fract. Eng. Mater. Struct.* **2001**, *24*, 105–116. [[CrossRef](#)]
64. Santos, T.F.; Marinho, R.R.; Paes, M.T.; Ramirez, A.J. Microstructure evaluation of UNS S32205 duplex stainless steel friction stir welds. *Rem Rev. Esc. Minas* **2013**, *66*, 187–191. [[CrossRef](#)]
65. Kasper, J. The ordering of atoms in the chi-phase of the iron-chromium-molybdenum system. *Acta Metall.* **1954**, *2*, 456–461. [[CrossRef](#)]
66. Byun, S.H.; Kang, N.; Lee, T.H.; Ahn, S.K.; Lee, H.W.; Chang, W.S.; Cho, K.M. Kinetics of Cr/Mo-rich precipitates formation for 25Cr-6.9Ni-3.8Mo-0.3N super duplex stainless steel. *Met. Mater. Int.* **2012**, *18*, 201–207. [[CrossRef](#)]
67. Kim, S.M.; Kim, J.S.; Kim, K.T.; Park, K.T.; Lee, C.S. Effect of Ce addition on secondary phase transformation and mechanical properties of 27Cr-7Ni hyper duplex stainless steels. *Mater. Sci. Eng. A* **2013**, *573*, 27–36. [[CrossRef](#)]
68. Hsieh, C.C.; Wu, W. Overview of intermetallic sigma (σ) phase precipitation in stainless steels. *ISRN Metall.* **2012**, *2012*, 16. [[CrossRef](#)]
69. Vinoth Jebaraj, A.; Ajaykumar, L. Influence of microstructural changes on impact toughness of weldment and base metal of duplex stainless steel AISI 2205 for low temperature applications. *Procedia Eng.* **2013**, *64*, 456–466. [[CrossRef](#)]
70. Wu, H.; Tsay, L.; Chen, C. Laser beam welding of 2205 duplex stainless steel with metal powder additions. *ISIJ Int.* **2004**, *44*, 1720–1726. [[CrossRef](#)]

71. Kingklang, S.; Uthaisangsuk, V. Investigation of hot deformation behavior of duplex stainless steel grade 2507. *Metall. Mater. Trans. A* **2016**, *48*, 95–108. [[CrossRef](#)]
72. Deng, B.; Jiang, Y.; Xu, J.; Sun, T.; Gao, J.; Zhang, L.; Zhang, W.; Li, J. Application of the modified electrochemical potentiodynamic reactivation method to detect susceptibility to intergranular corrosion of a newly developed lean duplex stainless steel LDX2101. *Corros. Sci.* **2010**, *52*, 969–977. [[CrossRef](#)]
73. Chan, K.W.; Tjong, S.C. Effect of secondary phase precipitation on the corrosion behavior of duplex stainless steels. *Materials* **2014**, *7*, 5268–5304. [[CrossRef](#)]
74. Ajith, P.M.; Sathiya, P.; Aravindan, S. Characterization of microstructure, toughness, and chemical composition of friction-welded joints of UNS S32205 duplex stainless steel. *Friction* **2014**, *2*, 82–91. [[CrossRef](#)]
75. Jinlong, L.; Tongxiang, L.; Limin, D.; Chen, W. Influence of sensitization on microstructure and passive property of AISI 2205 duplex stainless steel. *Corros. Sci.* **2016**, *104*, 144–151. [[CrossRef](#)]
76. Chasse, K.R.; Singh, P.M. Hydrogen embrittlement of a duplex stainless steel in alkaline sulfide solution. *Corrosion* **2011**, *67*, 015002-1–015002-12. [[CrossRef](#)]
77. Guo, Y.; Hu, J.; Li, J.; Jiang, L.; Liu, T.; Wu, Y. Effect of annealing temperature on the mechanical and corrosion behavior of a newly developed novel lean duplex stainless steel. *Materials* **2014**, *7*, 6604–6619. [[CrossRef](#)]
78. Sridhar, N.; Tormoen, G.; Hackney, S.; Anderko, A. Effect of aging treatments on the repassivation potential of duplex stainless steel S32205. *Corrosion* **2009**, *65*, 650–662. [[CrossRef](#)]
79. Geng, S.; Sun, J.; Guo, L.; Wang, H. Evolution of microstructure and corrosion behavior in 2205 duplex stainless steel GTA-welding joint. *J. Manuf. Process.* **2015**, *19*, 32–37. [[CrossRef](#)]
80. Schmidt-Rieder, E.; Tong, X.; Farr, J.; Aindow, M. In situ electrochemical scanning probe microscopy corrosion studies on duplex stainless steel in aqueous NaCl solutions. *Br. Corros. J.* **2013**, *31*, 139–146. [[CrossRef](#)]
81. Ramkumar, K.D.; Thiruvengatam, G.; Sudharsan, S.; Mishra, D.; Arivazhagan, N.; Sridhar, R. Characterization of weld strength and impact toughness in the multi-pass welding of super-duplex stainless steel UNS 32750. *Mater. Des.* **2014**, *60*, 125–135. [[CrossRef](#)]
82. Arikan, M.E.; Arikan, R.; Doruk, M. Determination of susceptibility to intergranular corrosion of UNS 31803 type duplex stainless steel by electrochemical reactivation method: A comparative study. *Int. J. Corros.* **2012**, *2012*, 1–14. [[CrossRef](#)]
83. Zhan, X.; Dong, Z.; Wei, Y.; Ma, R. Simulation of grain morphologies and competitive growth in weld pool of Ni–Cr alloy. *J. Cryst. Growth* **2009**, *311*, 4778–4783. [[CrossRef](#)]
84. Łabanowski, J.; Świerczyńska, A.; Topolska, S. Effect of microstructure on mechanical properties and corrosion resistance of 2205 duplex stainless steel. *Pol. Marit. Res.* **2014**, *21*, 108–112. [[CrossRef](#)]
85. Bermejo, M.V.; Karlsson, L.; Svensson, L.E.; Hurtig, K.; Rasmuson, H.; Frodigh, M.; Bengtsson, P. Effect of shielding gas on welding performance and properties of duplex and superduplex stainless steel welds. *Weld. World* **2015**, *59*, 239–249. [[CrossRef](#)]
86. Hazra, M.; Rao, K.S.; Reddy, G.M. Friction welding of a nickel free high nitrogen steel: Influence of forge force on microstructure, mechanical properties and pitting corrosion resistance. *J. Mater. Res. Technol.* **2014**, *3*, 90–100. [[CrossRef](#)]
87. Cárcel-Carrasco, F.J.; Pascual-Guillamón, M.; Pérez-Puig, M.A. Effects of X-rays radiation on AISI 304 stainless steel weldings with AISI 316L filler material: A study of resistance and pitting corrosion behavior. *Metals* **2016**, *6*, 102. [[CrossRef](#)]
88. Neissi, R.; Shamanian, M.; Hajihashemi, M. The effect of constant and pulsed current gas tungsten arc welding on joint properties of 2205 duplex stainless steel to 316L austenitic stainless steel. *J. Mater. Eng. Perform.* **2016**, *25*, 2017–2028. [[CrossRef](#)]
89. El-Batahgy, A.M.; Khourshid, A.F.; Sharef, T. Effect of laser beam welding parameters on microstructure and properties of duplex stainless steel. *Mater. Sci. Appl.* **2011**, *2*, 1443–1451. [[CrossRef](#)]
90. Mohammed, G.R.; Ishak, M.; Aqida, S.N.; Abdulhadi, H.A. The effect of fiber laser parameters on microhardness and microstructure of duplex stainless steel. *MATEC Web Conf.* **2017**, *90*, 01024. [[CrossRef](#)]
91. Srinivasan, P.B.; Muthupandi, V.; Dietzel, W.; Sivan, V. An assessment of impact strength and corrosion behaviour of shielded metal arc welded dissimilar weldments between UNS 31803 and IS 2062 steels. *Mater. Des.* **2006**, *27*, 182–191. [[CrossRef](#)]
92. Lothongkum, G.; Wongpanya, P.; Morito, S.; Furuhashi, T.; Maki, T. Effect of nitrogen on corrosion behavior of 28Cr–7Ni duplex and microduplex stainless steels in air-saturated 3.5 wt% NaCl solution. *Corros. Sci.* **2006**, *48*, 137–153. [[CrossRef](#)]

93. Yasuda, K.; Kimura, M.; Kawasaki, H.; Works, C.; Uegaki, T. Optimizing welding condition for excellent corrosion resistance in duplex stainless steel linepipe. *Kawasaki Steel Giho* **1988**, *20*, 197–202.
94. Jiang, Y.; Tan, H.; Wang, Z.; Hong, J.; Jiang, L.; Li, J. Influence of Cr_{eq}/Ni_{eq} on pitting corrosion resistance and mechanical properties of UNS S32304 duplex stainless steel welded joints. *Corros. Sci.* **2013**, *70*, 252–259. [[CrossRef](#)]
95. Moura, V.S.; Lima, L.D.; Pardal, J.M.; Kina, A.Y.; Corte, R.R.A.; Tavares, S.S.M. Influence of microstructure on the corrosion resistance of the duplex stainless steel UNS S31803. *Mater. Charact.* **2008**, *59*, 1127–1132. [[CrossRef](#)]
96. Sadeghian, M.; Shamanian, M.; Shafyei, A. Effect of heat input on microstructure and mechanical properties of dissimilar joints between super duplex stainless steel and high strength low alloy steel. *Mater. Des.* **2014**, *60*, 678–684. [[CrossRef](#)]
97. Lundquist, B.; Norberg, P.; Olsson, K. Influence of different welding conditions on mechanical properties and corrosion resistance of sandvik SAF 2205 (UNS S31803). In Proceedings of the Conference Duplex Stainless Steels, the Hague, Netherlands, October 1986; pp. 16–29.
98. Łabanowski, J. Mechanical properties and corrosion resistance of dissimilar stainless steel welds. *Arch. Mater. Sci. Eng.* **2007**, *28*, 27–33.
99. Hosseini, V.A.; Bermejo, M.A.V.; Gårdstam, J.; Hurtig, K.; Karlsson, L. Influence of multiple thermal cycles on microstructure of heat-affected zone in TIG-welded super duplex stainless steel. *Weld. World* **2016**, *60*, 233–245. [[CrossRef](#)]
100. Busschaert, F.; Cassagne, T.; Pedersen, A.; Johnsen, S. New challenges for the use of duplex stainless steels at low temperatures. *Rev. Metall.* **2013**, *110*, 185–197. [[CrossRef](#)]
101. Jang, S.H.; Kim, S.T.; Lee, I.S.; Park, Y.S. Effect of shielding gas composition on phase transformation and mechanism of pitting corrosion of hyper duplex stainless steel welds. *Mater. Trans.* **2011**, *52*, 1228–1236. [[CrossRef](#)]
102. Hosseini, V.A.; Wessman, S.; Hurtig, K.; Karlsson, L. Nitrogen loss and effects on microstructure in multipass TIG welding of a super duplex stainless steel. *Mater. Des.* **2016**, *98*, 88–97. [[CrossRef](#)]
103. Wang, S.; Ma, Q.; Li, Y. Characterization of microstructure, mechanical properties and corrosion resistance of dissimilar welded joint between 2205 duplex stainless steel and 16MnR. *Mater. Des.* **2011**, *32*, 831–837. [[CrossRef](#)]
104. Yang, L.; Zhang, Z.Z. Study on Weldability of Dissimilar Steel between 16MnR and S31803. *Adv. Mater. Res.* **2012**, *391–392*, 768–772. [[CrossRef](#)]
105. Tavares, S.; Pardal, J.; Lima, L.; Bastos, I.; Nascimento, A.; de Souza, J. Characterization of microstructure, chemical composition, corrosion resistance and toughness of a multipass weld joint of superduplex stainless steel UNS S32750. *Mater. Charact.* **2007**, *58*, 610–616. [[CrossRef](#)]
106. Olsson, C.O.A.; Landolt, D. Passive films on stainless steels—chemistry, structure and growth. *Electrochim. Acta* **2003**, *48*, 1093–1104. [[CrossRef](#)]
107. Kotecki, D.J. Some pitfalls in welding of duplex stainless steels. *Soldag. Insp.* **2010**, *15*, 336–343. [[CrossRef](#)]
108. Dong, W.; Kokawa, H.; Sato, Y.S.; Tsukamoto, S. Nitrogen desorption by high-nitrogen steel weld metal during CO₂ laser welding. *Metall. Mater. Trans. B* **2005**, *36*, 677–681. [[CrossRef](#)]
109. Lin, C.-M.; Tsai, H.-L.; Cheng, C.-D.; Yang, C. Effect of repeated weld-repairs on microstructure, texture, impact properties and corrosion properties of AISI 304L stainless steel. *Eng. Fail. Anal.* **2012**, *21*, 9–20. [[CrossRef](#)]
110. Lu, Z.; Shoji, T.; Meng, F.; Xue, H.; Qiu, Y.; Takeda, Y.; Negishi, K. Characterization of microstructure and local deformation in 316NG weld heat-affected zone and stress corrosion cracking in high temperature water. *Corros. Sci.* **2011**, *53*, 1916–1932. [[CrossRef](#)]
111. Lu, Z.; Shoji, T.; Xue, H.; Meng, F.; Fu, C.; Takeda, Y.; Negishi, K. Synergistic effects of local strain-hardening and dissolved oxygen on stress corrosion cracking of 316NG weld heat-affected zones in simulated BWR environments. *J. Nuclear Mater.* **2012**, *423*, 28–39. [[CrossRef](#)]
112. Yousefieh, M.; Shamanian, M.; Saatchi, A. Influence of heat input in pulsed current GTAW process on microstructure and corrosion resistance of duplex stainless steel welds. *J. Iron Steel Res. Int.* **2011**, *18*, 65–69. [[CrossRef](#)]
113. Gideon, B.; Ward, L.; Biddle, G. Duplex stainless steel welds and their susceptibility to intergranular corrosion. *J. Miner. Mater. Charact. Eng.* **2008**, *7*, 247–263. [[CrossRef](#)]

114. Tan, H.; Wang, Z.; Jiang, Y.; Yang, Y.; Deng, B.; Song, H.; Li, J. Influence of welding thermal cycles on microstructure and pitting corrosion resistance of 2304 duplex stainless steels. *Corros. Sci.* **2012**, *55*, 368–377. [[CrossRef](#)]
115. Silva, E.; Marinho, L.; Filho, P.; Leite, J.; Leite, J.; Fialho, W.; de Albuquerque, V.; Tavares, J. Classification of induced magnetic field signals for the microstructural characterization of sigma phase in duplex stainless steels. *Metals* **2016**, *6*, 164. [[CrossRef](#)]
116. Shimada, M.; Kokawa, H.; Wang, Z.; Sato, Y.; Karibe, I. Optimization of grain boundary character distribution for intergranular corrosion resistant 304 stainless steel by twin-induced grain boundary engineering. *Acta Mater.* **2002**, *50*, 2331–2341. [[CrossRef](#)]
117. Lin, S.X.; Bao, W.K.; Gao, J.; Wang, J.B. Intergranular Corrosion of Austenitic Stainless Steel. *Appl. Mech. Mater.* **2012**, 229–231, 14–17. [[CrossRef](#)]
118. Vlčková, I.; Jonšta, P.; Jonšta, Z.; Váňová, P.; Kulová, T. Corrosion fatigue of austenitic stainless steels for nuclear power engineering. *Metals* **2016**, *6*, 319. [[CrossRef](#)]
119. Mirshekari, G.R.; Tavakoli, E.; Atapour, M.; Sadeghian, B. Microstructure and corrosion behavior of multipass gas tungsten arc welded 304L stainless steel. *Mater. Des.* **2014**, *55*, 905–911. [[CrossRef](#)]
120. Tsai, W.T.; Chen, M.S. Stress corrosion cracking behavior of 2205 duplex stainless steel in concentrated nacl solution. *Corros. Sci.* **2000**, *42*, 545–559. [[CrossRef](#)]
121. Kim, K.; Zhang, P.; Ha, T.; Lee, Y. Electrochemical and stress corrosion properties of duplex stainless steels modified with tungsten addition. *Corrosion* **1998**, *54*, 910–921. [[CrossRef](#)]
122. Nilsson, J.O.; Kangas, P.; Wilson, A.; Karlsson, T. Mechanical properties, microstructural stability and kinetics of σ -phase formation in 29Cr-6Ni-2Mo-0.38N superduplex stainless steel. *Metall. Mater. Trans. A* **2000**, *31*, 35–45. [[CrossRef](#)]
123. Strubbia, R.; Hereñú, S.; Marinelli, M.; Alvarez-Armas, I. Short crack nucleation and growth in lean duplex stainless steels fatigued at room temperature. *Int. J. Fatigue* **2012**, *41*, 90–94. [[CrossRef](#)]
124. Brandolt, C.; Rosa, M.; Ramos, L.; Schroeder, R.; Malfatti, C.; Müller, I. Temperature influence on SCC behaviour of duplex stainless steel. *Mater. Sci. Technol.* **2016**, 1–7. [[CrossRef](#)]
125. Li, H.; Jiao, W.; Feng, H.; Li, X.; Jiang, Z.; Li, G.; Wang, L.; Fan, G.; Han, P. Deformation characteristic and constitutive modeling of 2707 hyper duplex stainless steel under hot compression. *Metals* **2016**, *6*, 223. [[CrossRef](#)]
126. Bellezze, T.; Giuliani, G.; Roventi, G.; Fratesi, R.; Andreatta, F.; Fedrizzi, L. Corrosion behaviour of austenitic and duplex stainless steels in an industrial strongly acidic solution. *Mater. Corros.* **2016**, *67*, 831–838. [[CrossRef](#)]
127. Tseng, C.M.; Tsai, W.T. Environmentally assisted cracking behavior of single and dual phase stainless steels in hot chloride solutions. *Mater. Chem. Phys.* **2004**, *84*, 162–170. [[CrossRef](#)]
128. El-Yazgi, A.; Hardie, D. Stress corrosion cracking of duplex and super duplex stainless steels in sour environments. *Corros. Sci.* **1998**, *40*, 909–930. [[CrossRef](#)]
129. Örnek, C.; Idris, S.A.; Reccagni, P.; Engelberg, D.L. Atmospheric-induced stress corrosion cracking of grade 2205 duplex stainless steel—Effects of 475 °C embrittlement and process orientation. *Metals* **2016**, *6*, 167. [[CrossRef](#)]
130. Chattoraj, I. Stress Corrosion Cracking of Duplex Stainless Steels. *Adv. Mater. Res.* **2013**, *794*, 552–563. [[CrossRef](#)]
131. Bhattacharya, A.; Singh, P.M. Effect of heat treatment on corrosion and stress corrosion cracking of S32205 duplex stainless steel in caustic solution. *Metall. Mater. Trans. A* **2009**, *40*, 1388–1399. [[CrossRef](#)]
132. Muthupandi, V.; Bala Srinivasan, P.; Seshadri, S.K.; Sundaresan, S. Effect of weld metal chemistry and heat input on the structure and properties of duplex stainless steel welds. *Mater. Sci. Eng. A* **2003**, *358*, 9–16. [[CrossRef](#)]
133. Esmailzadeh, M.; Shamanian, M.; Kermanpur, A.; Saeid, T. Microstructure and mechanical properties of friction stir welded lean duplex stainless steel. *Mater. Sci. Eng. A* **2013**, *561*, 486–491. [[CrossRef](#)]
134. Reddy, G.M.; Rao, K.S. Microstructure and mechanical properties of similar and dissimilar stainless steel electron beam and friction welds. *Int. J. Adv. Manuf. Technol.* **2009**, *45*, 875–888. [[CrossRef](#)]
135. Kordatos, J.; Fourlaris, G.; Papadimitriou, G. The effect of cooling rate on the mechanical and corrosion properties of SAF 2205 (UNS 31803) duplex stainless steel welds. *Scr. Mater.* **2001**, *44*, 401–408. [[CrossRef](#)]

136. Calliari, I.; Straffellini, G.; Ramous, E. Investigation of secondary phase effect on 2205 DSS fracture toughness. *Mater. Sci. Technol.* **2010**, *26*, 81–86. [[CrossRef](#)]
137. Ibrahim, O.; Ibrahim, I.; Khalifa, T. Impact behavior of different stainless steel weldments at low temperatures. *Eng. Fail. Anal.* **2010**, *17*, 1069–1076. [[CrossRef](#)]
138. Kumar, S.; Shahi, A.S. On the influence of welding stainless steel on microstructural development and mechanical performance. *Mater. Manuf. Process.* **2014**, *29*, 894–902. [[CrossRef](#)]
139. Song, T.; Jiang, X.; Shao, Z.; Mo, D.; Zhu, D.; Zhu, M. The interfacial microstructure and mechanical properties of diffusion-bonded joints of 316L stainless steel and the 4J29 kovar alloy using nickel as an interlayer. *Metals* **2016**, *6*, 263. [[CrossRef](#)]
140. Mourad, A.H.I.; Khourshid, A.; Sharef, T. Gas tungsten arc and laser beam welding processes effects on duplex stainless steel 2205 properties. *Mater. Sci. Eng. A* **2012**, *549*, 105–113. [[CrossRef](#)]
141. Shrikrishna, K.A.; Sathiya, P. Effects of post weld heat treatment on friction welded duplex stainless steel joints. *J. Manuf. Process.* **2015**, *21*, 196–200.
142. Atapour, M.; Sarlak, H.; Esmailzadeh, M. Pitting corrosion susceptibility of friction stir welded lean duplex stainless steel joints. *Int. J. Adv. Manuf. Technol.* **2015**, *83*, 721–728. [[CrossRef](#)]
143. Abdulhadi, H.A.; Aqida, S.N.; Ishak, M.; Mohammed, G.R. Thermal fatigue of die-casting dies: An overview. *MATEC Web Conf.* **2016**, *74*, 00032. [[CrossRef](#)]
144. Chagas de Souza, G.; da Silva, A.L.; Tavares, S.S.M.; Pardal, J.M.; Ferreira, M.L.R.; Filho, I.C. Mechanical properties and corrosion resistance evaluation of superduplex stainless steel UNS S32760 repaired by gtaw process. *Weld. Int.* **2016**, *30*, 432–442. [[CrossRef](#)]



© 2017 by the authors; licensee MDPI, Basel, Switzerland. This article is an open access article distributed under the terms and conditions of the Creative Commons Attribution (CC BY) license (<http://creativecommons.org/licenses/by/4.0/>).